Biophysical Letter

Reversible Effects of Peptide Concentration and Lipid Composition on H-Ras Lipid Anchor Clustering

Xubo Lin,[1] Zhenlong Li,[1] and Alemayehu A. Gorfe[1,*]
[1]Department of Integrative Biology and Pharmacology, Medical School, The University of Texas Health Science Center at Houston, Houston, Texas

ABSTRACT Dynamic clusters of lipid-anchored Ras proteins are important for high-fidelity signal transduction in cells. The average size of Ras nanoclusters was reported to be independent of protein expression levels, and cholesterol depletion is commonly used to test the raft-preference of nanoclusters. However, whether protein concentration and membrane domain stability affect Ras clustering in a reversible manner is not well understood. We used coarse-grained molecular dynamics simulations to examine the reversibility of the effects of peptide and cholesterol concentrations as well as a lipid domain-perturbing nanoparticle (C_{60}) on the dynamics and stability of H-Ras lipid-anchor nanoclusters. By comparing results from these simulations with previous observations from the literature, we show that effects of peptide/cholesterol concentrations on the dynamics and stability of H-Ras peptide nanoclusters are reversible. Our results also suggest a correlation between the stabilities of lipid domains and Ras nanoclusters, which is supported by our finding that C_{60} penetrates into the liquid-disordered domain of the bilayer, destabilizing lipid domains and thereby the stability of the nanoclusters.

Received for publication 7 July 2015 and in final form 6 November 2015.

*Correspondence: alemayehu.g.abebe@uth.tmc.edu

Previous experiments have shown that Ras proteins assemble into dynamic nanoclusters on the plasma membrane (PM) (1), as well as in synthetic model membranes (2,3). Nanoclustering is essential for the biological function of Ras proteins, which mediates signal transduction pathways involved in cell growth and development (4). Somatic mutations that lead to unregulated Ras function are found in 15–25% of all human cancers (4). There are three common Ras proteins in humans (namely, H-, N-, and K-Ras A/B) that share a highly conserved catalytic domain but differ at the C-terminus, where they undergo posttranslational lipid modification(s) before binding to the PM (1). The minimal PM anchor of H-Ras, a farnesylated and doubly palmitoylated heptapeptide (tH), forms nanoclusters similar to the full-length protein (5). Therefore, tH is an excellent model system to study Ras clustering in atomic detail.

Recently, we used coarse-grained (CG) molecular dynamics (MD) simulations to show that (6–8): 1) tH nanoclusters in model bilayers predominantly localize at the interface between liquid-ordered (L_o) and liquid-disordered (L_d) domains and modulate bilayer curvature; 2) there is a critical concentration below which tH does not form clusters; and 3) cholesterol stabilizes lipid domains and thereby tH nanoclusters, but it is not required for cluster formation. However, it was not clear whether these are reversible processes. Reversibility has important implications on the apparent independence of the average size of Ras nanoclusters on protein expression levels (1,5) and the relevance of cholesterol depletion (e.g., by methyl-β-cyclodextrin (9) treatment) to test raft-preference of nanoclusters. Reversibility is also crucial for the regulation of Ras function through nanocluster dynamics (10). Here we studied, with the same CG MD approach we have used previously, possible declustering or changes in the stability/dynamics of preformed tH nanoclusters upon a systematic depletion of tH and cholesterol from a system containing clustered tH. Our goal is to test whether effects of peptide and cholesterol concentration on nanocluster size, stability, and lateral distribution are reversible.

We used the MARTINI CG model (Ver. 2.1) (11) and the GROMACS program (Ver. 4.5.4) (12) for all of these simulations (see Table S1 in the Supporting Material), which were started from a snapshot at 32 μs of a previous simulation (7) on a bilayer composed of 960 DPPC (dipalmitoylphosphatidylcholine), 576 DLiPC (dilinoleoylphosphatidylcholine), 576 cholesterol, 64 tH, and 17,789 water molecules plus 128 Na^+ and 192 Cl^- ions. The 64 tH molecules were all on one leaflet to mimic Ras binding to the inner leaflet of the PM. Of these, we deleted 0, 16, 32, and 48 tH molecules from the nonclustered fraction (monomer, dimers, or trimers; see Janosi et al. (6) and Li et al. (7)) to examine the effect of decreasing tH concentration on clustering; nanoclusters of size 4 or higher were left intact to allow for

Editor: Scott Feller.

http://dx.doi.org/10.1016/j.bpj.2015.11.009

potential spontaneous declustering. Similarly, we studied the impact of cholesterol depletion by deleting 0, 192, 384, and 576 cholesterol molecules (half from each leaflet), resulting in 27, 20, 11, and 0% cholesterol systems while keeping the number of tH fixed at 64. Subsequent steps of system equilibration, production, and data analysis were identical to previous work (6,7); a brief description is provided in the Supporting Material.

Results from the simulations with decreasing tH concentration are summarized in Figs. 1 and S5 *a*. They show that tH depletion did not lead to changes in lipid domain organization; both the DPPC/cholesterol-enriched L_o and DLiPC-enriched L_d domains remained intact (Fig. 1, *a* and *b*). However, there is significant variation between the smallest tH concentration (16 tH) and the rest in terms of tH cluster size distribution (Fig. 1 *c*), especially in the fraction of aggregates of size 4 or higher that represent nanoclusters based on our previous definition (6,7). Specifically, the cluster size distributions before tH depletion (i.e., with 64 tH) and after removal of 25 and 50% of the peptides are similar, but further reduction to 16 peptides led to negligible nanoclustering. This is consistent with our previous estimate that a peptide/lipid of ~1:100 might be required for cluster formation (7). Moreover, projection of the center-of-mass positions of tH molecules on a two-dimensional heat map of the mean DPPC positions shows that the peptides frequently sample the interface between the L_o and L_d domains. The same observation has been made in our previous studies (6,7). We conclude that the effect of peptide concentration on tH nanoclustering is reversible. Although not the main focus of this study, we note that asymmetric tH insertion could cause curvature to the bilayer (6–8); however, this does not have adverse effect on clustering (Fig. S1).

We previously showed that increasing cholesterol concentration enhances the stability of tH nanoclusters but does not significantly affect their formation or size distribution (7). This suggested that cholesterol is not required for tH clustering, but is important for stability (7). We hypothesized that is a reversible process; namely, decreasing cholesterol concentration in a system of preformed tH nanoclusters would have a similar effect as increasing cholesterol before clustering. To test this hypothesis, we ran four simulations with progressively lower cholesterol content (27, 20, 11, and 0%), all started from a previously simulated bilayer system containing a fixed number of 64 tH molecules. The reduction in cholesterol fraction led to progressively increasing lipid mixing (Fig. 2 *a*), but the size distribution of the tH clusters remained almost unaffected (Figs. 2 *b* and S5 *b*). This result not only confirms our previous observation that cholesterol is not required for tH clustering, but also indicates that cholesterol depletion does not decluster tH. On the other hand, analysis of the rate of decay of selected clusters (Fig. 2 *c*) in terms of a molecular expulsion autocorrelation function $f(t)$ described in the Supporting Material suggest that cholesterol depletion increases cluster dynamics and, thereby, the rate of exchange between the pools of clustered and nonclustered fractions. Combined with our previous observations (7), these results strongly suggest that cholesterol depletion, despite being a common technique to test raft-preference of nanoclusters (9), does not lead to declustering. Instead, it reversibly affects cluster dynamics.

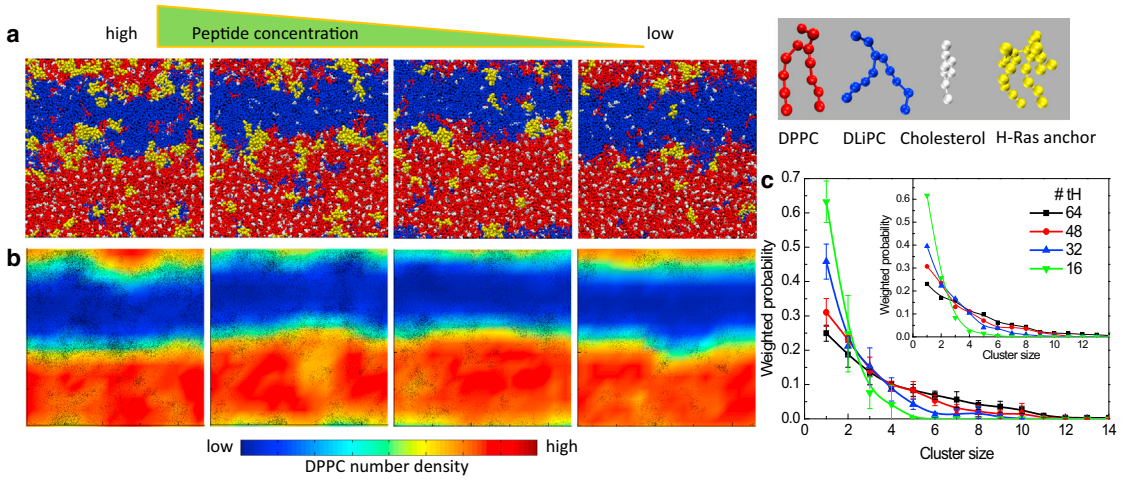

FIGURE 1 Effect of decreasing peptide concentration on tH clustering. (*a*, *left* to *right*) The last snapshot from a 12 μs trajectory of systems with 64, 48, 32, and 16 tH molecules (*color scheme* is the same as the molecular models, *right top*). (*b*, *left* to *right*) Two-dimensional number-density map of DPPC colored from low (*blue*) through high (*red*) and the instantaneous location of tH molecules (*black points*) derived from analysis of each of the last 4 μs trajectories. (*c*) Probability distribution of tH cluster sizes upon reduction of tH molecules (*error bars* represent SD from averaging over eight 500 ns blocks of the last 4 μs of the 12 μs data; see Section S8 in the Supporting Material for details). (*Inset*) Results from one of the two additional simulations with different initial velocity assignments. To see this figure in color, go online.

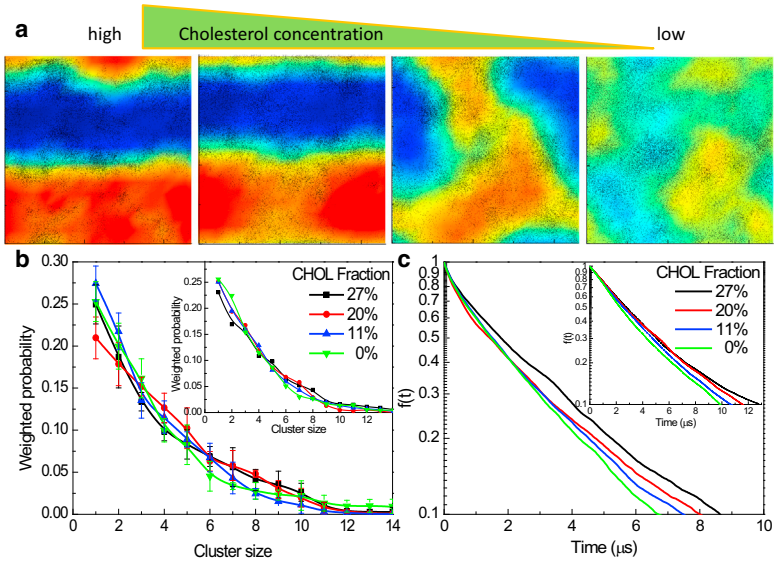

FIGURE 2 Cholesterol depletion reduces lipid domain stability and enhances tH cluster dynamics. (*a*, *left* to *right*) Two-dimensional number-density map of DPPC colored from low (*blue*) through high (*red*) along with the instantaneous location of tH molecules (*black points*) based on analysis over the last 4 μs trajectories. (*b*) Probability distribution of tH cluster sizes upon cholesterol depletion; error from averaging over eight 500-ns blocks of the last 4 μs of data. (*Inset*) Data from another independent set of simulations. (*c*) Stability of tH nanoclusters upon cholesterol depletion. Considering that on average there are ~6 Ras proteins per cluster (5), here we show *f*(*t*) for clusters of size 6, although *f*(*t*) values for other cluster sizes exhibit similar trends (as an example, the *inset* shows *f*(*t*) for cluster size 4). To see this figure in color, go online.

The results described above suggest a correlation between the stabilities of Ras nanoclusters and lipid domains (i.e., extent of lipid demixing). It follows that compounds that directly or indirectly affect lipid domain stability might also affect protein clustering. To test this hypothesis, we used a nanoparticle (C_{60}) as a perturbant of domain integrity because it has been shown to partition to the L_d phase of multidomain bilayers (13). C_{60} belongs to a class of biomedically relevant (e.g., as drug-delivery vehicles) carbon-based nanoparticles whose interaction with biomembranes is the subject of intense investigations. We simulated the 64-tH/27% cholesterol system after adding an aggregate of 16 C_{60} molecules into the water box. Consistent with previous reports (13), we found that the C_{60} aggregate quickly adheres to the bilayer, enters into the hydrophobic core of the L_d domain, and dissolves into individual C_{60} molecules (Fig. S4, *a* and *b*). This led to significant lipid remixing and thus destabilization of the striped lipid domains (Fig. S4 *c*). Consequently, the stability/dynamics of tH clusters was altered in a manner that is similar to cholesterol depletion (Figs. S4 *e* and 2 *c*). Also, just as cholesterol depletion did not decluster tH, the size distribution of tH clusters was not significantly affected by the presence of C_{60} (see Fig. S4 *d*). These results support our conclusion that the stability (and lateral distribution) of tH clusters is a function of the stability of lipid domains.

In summary, previous experiments have shown that Ras nanoclusters are important for high-fidelity signal transduction (10) while MD studies provided detailed information about the driving forces for Ras clustering in model lipid bilayers (6,7). Here we examined the effects of peptide and cholesterol depletion on the dynamics and stability of the H-Ras lipid anchor nanoclusters using a tens-of-microseconds timescale CG MD. As summarized in Fig. S5, we found that the effect of systematic depletion of the nonclustered tH fraction is equivalent to increasing tH concentration. Similarly, depletion of cholesterol destabilizes lipid domains and thereby the stability of tH clusters, but it has no effect on cluster formation per se. We conclude that effects of changes in both peptide and cholesterol concentration are reversible. Additional evidence for the correlation between the stabilities of lipid domains and tH clusters was provided by C_{60}, which partitioned into the core of the L_d domain and destabilized lipid domains as well as tH nanoclusters.

SUPPORTING MATERIAL

Supporting Material, six figures, two tables, and simulation and analysis details are available at http://www.biophysj.org/biophysj/supplemental/S0006-3495(15)01166-2.

AUTHOR CONTRIBUTIONS

A.A.G. and X.L. designed research; X.L. and Z.L. performed research; X.L., A.A.G., and Z.L. analyzed data; and X.L. and A.A.G. wrote the article.

ACKNOWLEDGMENTS

We thank the National Institutes of Health (grant No. RO1 GM100078) for financial support and the Texas Advanced Computing Center for computational resources.

REFERENCES

1. Abankwa, D., A. A. Gorfe, and J. F. Hancock. 2007. Ras nanoclusters: molecular structure and assembly. *Semin. Cell Dev. Biol.* 18:599–607.
2. Weise, K., G. Triola, …, R. Winter. 2009. Influence of the lipidation motif on the partitioning and association of N-Ras in model membrane subdomains. *J. Am. Chem. Soc.* 131:1557–1564.
3. Weise, K., S. Kapoor, …, R. Winter. 2011. Membrane-mediated induction and sorting of K-Ras microdomain signaling platforms. *J. Am. Chem. Soc.* 133:880–887.

4. Cox, A. D., S. W. Fesik, …, C. J. Der. 2014. Drugging the undruggable RAS: mission possible? *Nat. Rev. Drug Discov.* 13:828–851.

5. Zhou, Y., and J. F. Hancock. 2015. Ras nanoclusters: versatile lipid-based signaling platforms. *Biochim. Biophys. Acta Mol. Cell Res.* 1853:841–849.

6. Janosi, L., Z. Li, …, A. A. Gorfe. 2012. Organization, dynamics, and segregation of Ras nanoclusters in membrane domains. *Proc. Natl. Acad. Sci. USA.* 109:8097–8102.

7. Li, Z., L. Janosi, and A. A. Gorfe. 2012. Formation and domain partitioning of H-Ras peptide nanoclusters: effects of peptide concentration and lipid composition. *J. Am. Chem. Soc.* 134:17278–17285.

8. Li, Z., and A. A. Gorfe. 2013. Deformation of a two-domain lipid bilayer due to asymmetric insertion of lipid-modified Ras peptides. *Soft Matter.* 9:11249–11256.

9. Niv, H., O. Gutman, …, Y. I. Henis. 2002. Activated K-Ras and H-Ras display different interactions with saturable nonraft sites at the surface of live cells. *J. Cell Biol.* 157:865–872.

10. Tian, T., A. Harding, …, J. F. Hancock. 2007. Plasma membrane nanoswitches generate high-fidelity Ras signal transduction. *Nat. Cell Biol.* 9:905–914.

11. Monticelli, L., S. K. Kandasamy, …, S. J. Marrink. 2008. The MARTINI coarse-grained force field: extension to proteins. *J. Chem. Theory Comput.* 4:819–834.

12. Hess, B., C. Kutzner, …, E. Lindahl. 2008. GROMACS 4: algorithms for highly efficient, load-balanced, and scalable molecular simulation. *J. Chem. Theory Comput.* 4:435–447.

13. Sun, D., X. Lin, and N. Gu. 2014. Cholesterol affects C_{60} translocation across lipid bilayers. *Soft Matter.* 10:2160–2168.

Supporting Material for

Reversible Effects of Peptide Concentration and Lipid Composition on H-Ras Lipid Anchor Clustering

X. Lin, Z. Li, and A. A. Gorfe*

Department of Integrative Biology and Pharmacology, Medical School, The University of Texas Health Science Center at Houston, Houston, Texas 77030, United States

* Corresponding author: E-mail: alemayehu.g.abebe@uth.tmc.edu

Contents

1. Lipid domain formation and effect of bilayer asymmetry on tH clustering

The simulations in the current work involved a bilayer of DPPC (dipalmitoylphosphatidylcholine), DLiPC (dilinoleoylphosphatidylcholine) and CHOL (cholesterol), with or without H-Ras lipid anchor (tH) embedded in one leaflet. To find a bilayer system capable of domain formation and to examine the effect of asymmetric tH insertion on clustering, we tested the three test systems listed in Table S1. As shown in Fig S1, simulation of these systems from a random initial mixture led to rapid (several μs) lipid de-mixing and formation of two striped domains (Fig S1a). One of these domains is enriched with DPPC and CHOL (liquid ordered domain, L_o), while the other is enriched with DLiPC (liquid disordered domain, L_d). The two domains differ by ~0.8nm in thickness (see Fig S1b).

Table S1: Summary of test simulations performed in this work[&]

System	Upper leaflet				Lower leaflet				Length (μs)
	DPPC	DLiPC	CHOL	tH	DPPC	DLiPC	CHOL	tH	
1	480	288	192	0	480	288	192	0	12
2	480	288	192	0	480	288	192	64	12
3	480	288	192	0	416	256	192	64	12

[&] Simulation details are as described in the following section; system 2 is the same as the 20% CHOL system discussed in the main text and in Table S2.

Note that we inserted tH only to the lower leaflet in order to mimic Ras binding to the inner leaflet of plasma membrane. This may cause inter-leaflet area asymmetry and curvature. A detailed analysis of this issue in previous work[1] showed that the total area of the leaflet with 64 tH molecules (the maximum number of tH used in the current study) was 563 nm^2 while that of the tH-free leaflet was 557 nm^2, resulting in a difference of only 6 nm^2 or 1.1% (see Fig 7a in ref. 1). This is because (i) the maximum fraction of tH relative to the total number of molecules in the bilayer is only 3.2%, and (ii) area mismatch is partially relieved by cholesterol re-distribution between leaflets (see Fig 6a in ref. 1). In one of the current simulations containing 64 asymmetrically bound tH (system 2), 74.6 ± 7.3 cholesterol molecules have transferred from the lower to the upper leaflet (see Fig. S2c).

Park *et al*[2] reported that area per lipid mismatch of up to 5% is tolerated in all-atom MD simulation of reasonably-sized (40-160 lipids per leaflet) bilayers. Assuming a direct correlation between total area and area per lipid, the ~1.1% inter-leaflet area mismatch in our system should not have significant effect on tH binding or clustering. Nevertheless, we directly tested the impact of area asymmetry on tH clustering by simulating a bilayer in which the overall surface area of the two leaflets was nearly the same. This was achieved by deleting 64 DPPC and 32 DLiPC lipids from the leaflet in which tH was bound. The number of deleted lipids was determined based on the work of Vogel *et al*.[3,4], who found that the average cross-sectional area of a saturated lipid tail of N-Ras varied between 0.236 nm^2 and 0.354 nm^2, depending on the chain length and saturation of the host bilayer. For a DPPC/CHOL

bilayer, the cross-secretion areas of N-Ras and DPPC lipid chains were similar (0.236 vs. 0.227 nm^2; table 1 of Vogel *et al*[3]). When the host bilayer was POPC, the cross-section of an N-Ras hydrocarbon tail is similar to that of POPC (0.333 vs. 0.306 nm^2). Since tH predominantly localizes at the lipid domain boundary so that--on the main--its two saturated lipids interact with the DPPC/CHOL domain and its unsaturated farnesyl tail with the DLiPC domain[5,6], we estimated that the total cross-section of 128 palmitoyl chains (64×2) would be roughly equal to the total area of 64 DPPC lipids (64×2 16:0 chains). Since the DLiPC-interacting farnesyl chain is more flexible, we estimated that the cross-section of 64 farnesyls would be equivalent to the area of 32 DLiPC lipids. Therefore, we deleted 64 DPPC and 32 DLiPC from the leaflet containing 64 tH molecules. Simulation of this system (system 3) yielded domain thicknesses (Fig. S1b), number of cholesterol/leaflet (Fig. S1c) and box area (Fig. S1d) that are comparable with those from a tH-free bilayer (system 1). More importantly, there was no significant difference between systems 3 and 2 in terms of lipid domain formation and structure (Fig. S1a, b), tH clustering profile (Fig. S1e, f) and even overall tH lateral distribution (Fig. S1a). These results demonstrate that, at least at the concentration regimes of the current work, asymmetric tH insertion faithfully models membrane binding of cellular Ras without adversely affecting cluster formation.

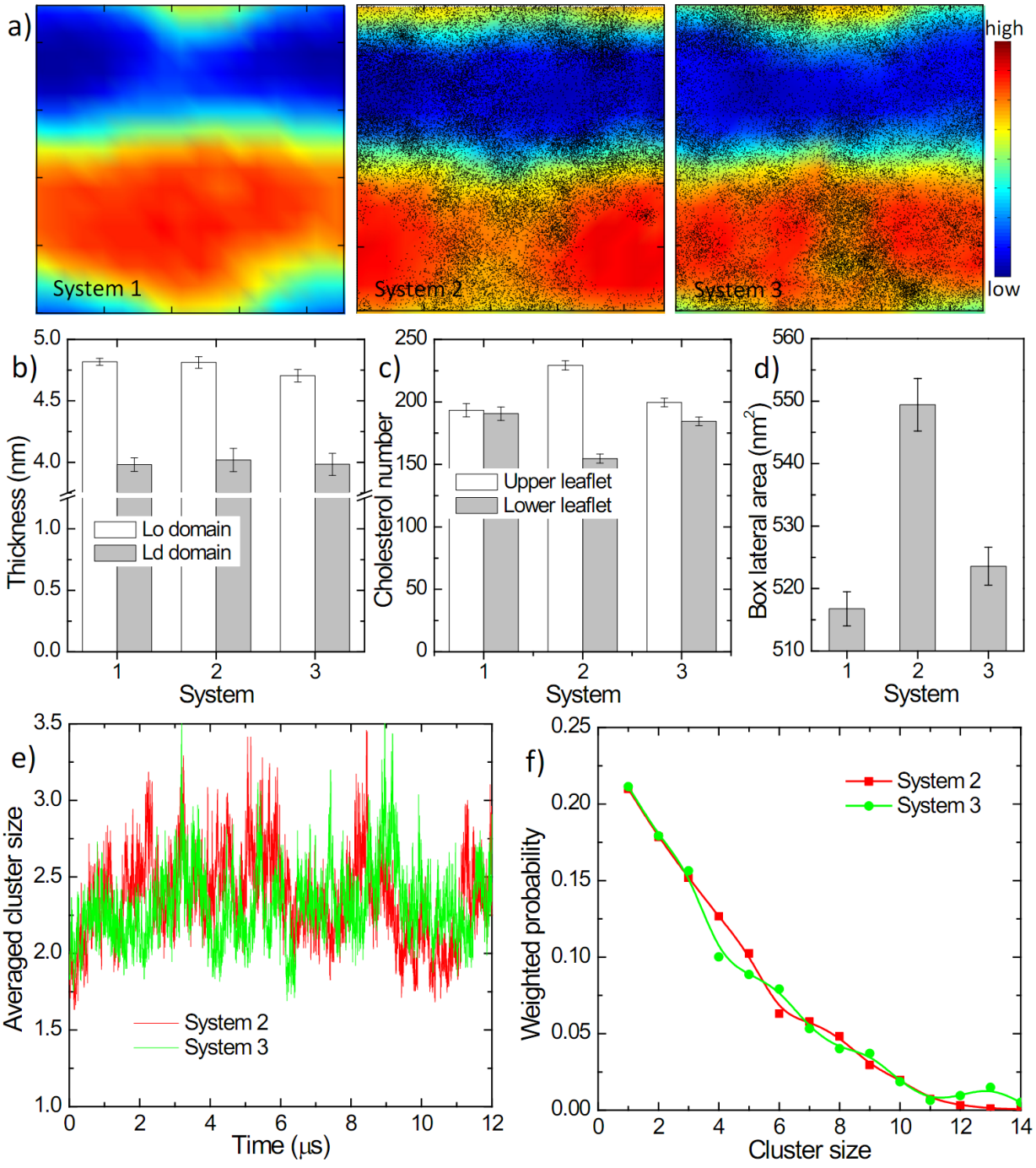

Figure S1. (a) Two-dimensional plots of average number density of DPPC (blue to red) and the location of tH molecules (black points); additional details can be found the in legend of Fig 1 in the main text. (b) Thicknesses of the L_o and L_d domains measured as the average inter-leaflet head-to-head distance based on the z-position of the PO4 beads of DPPC and DLiPC, respectively. To account for curvature and undulations, the thicknesses were calculated in 1nm-side slabs and averaged over the slabs. (c) Average number of cholesterol in each leaflet of the bilayer. (d) Average area of the simulation box in the x-y plane. (e-f) Time evolution of average cluster size (d) and probability distribution (f) of tH cluster sizes in systems 1 and 2. Except in (e), the last 4 μs of the trajectory was used; standard deviations are shown as error bars in (b), (c) and (d).

2. Simulation Details

In addition to the test systems referred to in the previous section, we simulated eight systems each in replicates of three (Table S2). In four of these the DPPC/DLiPC/CHOL ratio was kept fixed while the number of tH was progressively reduced as described in the main text. In the other four, the fraction of cholesterol was progressively decreased while keeping the number of peptides fixed at 64 (and always maintaining equal numbers of cholesterol in the two leaflets in the beginning). In every case, tH was asymmetrically bound to one leaflet, which, as shown above, has little impact on clustering. Following model building, each system was first (re)-equilibrated in two steps each of 100 ns duration. In the first step, tH, lipid and C_{60} (where applicable) molecules were position-restrained using a harmonic force constant of 1000 $kJ\ mol^{-1}\ nm^{-2}$. In the second step, the position restraint was applied only on tH. Subsequently, all restraints were removed and production simulations commenced for the durations shown in Table S2. In each simulation, the Lennard-Jones potentials describing van der Waals interactions were smoothly shifted to zero between 0.9 nm and 1.2 nm, Coulomb electrostatic interactions were truncated at 1.2 nm, and a default dielectric constant of 15 was used[7]. Lipids, H-Ras lipid anchors (tH), water and ions were coupled separately to V-rescale heat baths[8] at $T = 301K$ with a coupling constant $\tau = 1\ ps$. Constant number of particle, pressure and temperature (NPT ensemble) simulations were conducted at $1\ bar$ using semi-isotropic Parrinello-Rahman pressure coupling scheme[9] with a coupling constant $\tau = 5ps$ and a compressibility of $3\times10^{-4}\ bar^{-1}$. The neighbor list for non-bonded interactions was updated every 10 steps and the time step was 20 fs. A summary of the simulations performed in this work is presented in Table S1. We have used the 8-12 μs of each trajectory for the analysis of cluster size distribution as well as number of density of lipids, and the last 32 μs of each 40 μs trajectory for the analysis of long timescale processes such as molecular expulsion autocorrelation functions.

Table S2. Summary of investigative simulations performed in this study*.

System	Composition (number of molecules)					Length (μs)[§]
	DPPC	DLiPC	CHOL	tH	C_{60}	
$S_{64,27,0}$	960	576	576	64	0	40
$S_{48,27,0}$	960	576	576	48	0	12
$S_{32,27,0}$	960	576	576	32	0	12
$S_{16,27,0}$	960	576	576	16	0	12
$S_{64,20,0}$	960	576	384	64	0	40
$S_{64,11,0}$	960	576	192	64	0	40
$S_{64,0,0}$	960	576	0	64	0	40
$S_{64,27,16}$	960	576	576	64	16	40

- * $S_{a,b,c}$ represents the name of the system, where "a" is the number of tH molecules, "b" is the lipid fraction of cholesterol and "c" is the number of C_{60} nanoparticles. Simulation length is the effective time (4 × actual simulation length). The simulations were run for 12 μs for cases where we were only interested in cluster size distribution or 40 μs for cases where we were also interested in analyzing the compositional dynamics of tH nanoclusters whose relaxation time was relatively long (ref. 8, 9).
- [§] Each system was simulated in replicates of three with the second and third runs being 12 μs long. The results from the replicates were very similar (see main text) and therefore we used only one of the copies for most of the analysis.

3. Time evolution of average cluster sizes

Clustering was monitored by a Single-Linkage (SL) algorithm described previously[10-12], with neighbors defined based on a distance cutoff of 7.5 Å; this cutoff was derived from an analysis of two-dimensional pair distributions. Fig. S2 shows the time evolution of average cluster size.

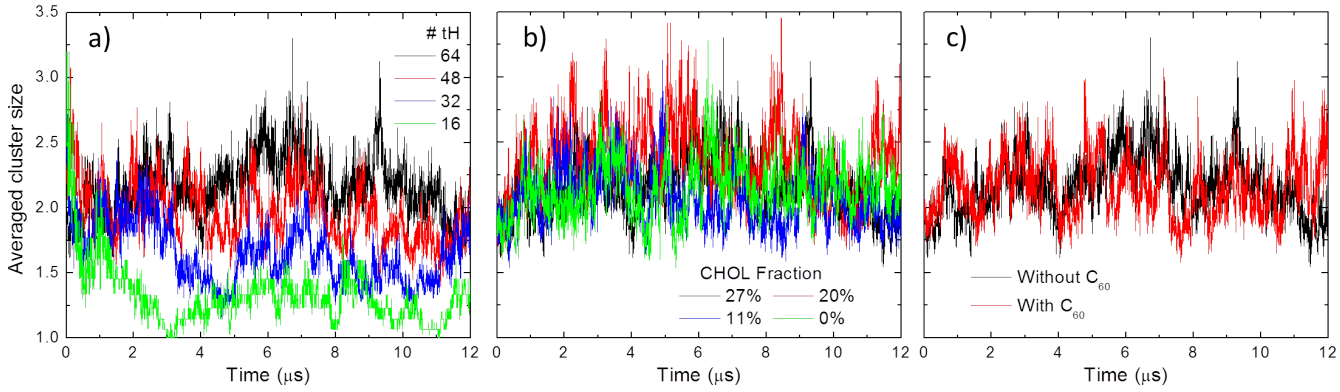

Figure S2. Time evolution of average cluster sizes during simulations with different peptide (a) and cholesterol (b) concentrations, and in the presence of C_{60} (c).

4. Error analysis

The error bars in Fig. 1c and 2b (main text) were calculated using averaging with a single 500ns block size over the last 4 μs of 12 μs trajectories. To check if this block size is reasonable, we divided the 4 μs trajectory into N_b blocks of progressively increasing size and evaluated the sampling error σ_b as

$$\sigma_b = \sqrt{\frac{1}{N_b}\sum_{i=1}^{N_b}(x_i - \bar{x})^2} \qquad (1)$$

where x_i and $\bar{x}$ are averages over block size i<4μs and 4μs, respectively. As shown in Fig. S3, larger block sizes result in smaller errors. In most cases, the errors for different cluster sizes and simulation conditions plateaued at about 400-600ns. The relatively large scattering for the larger clusters at larger block sizes reflects the diminishing number of samples (smaller N_b). We therefore chose a reasonable tradeoff of 500ns block size ($N_b = 8$) for estimation of the errors shown in Figs. 1 and 2 of the main text and section 7 of the Supporting Material.

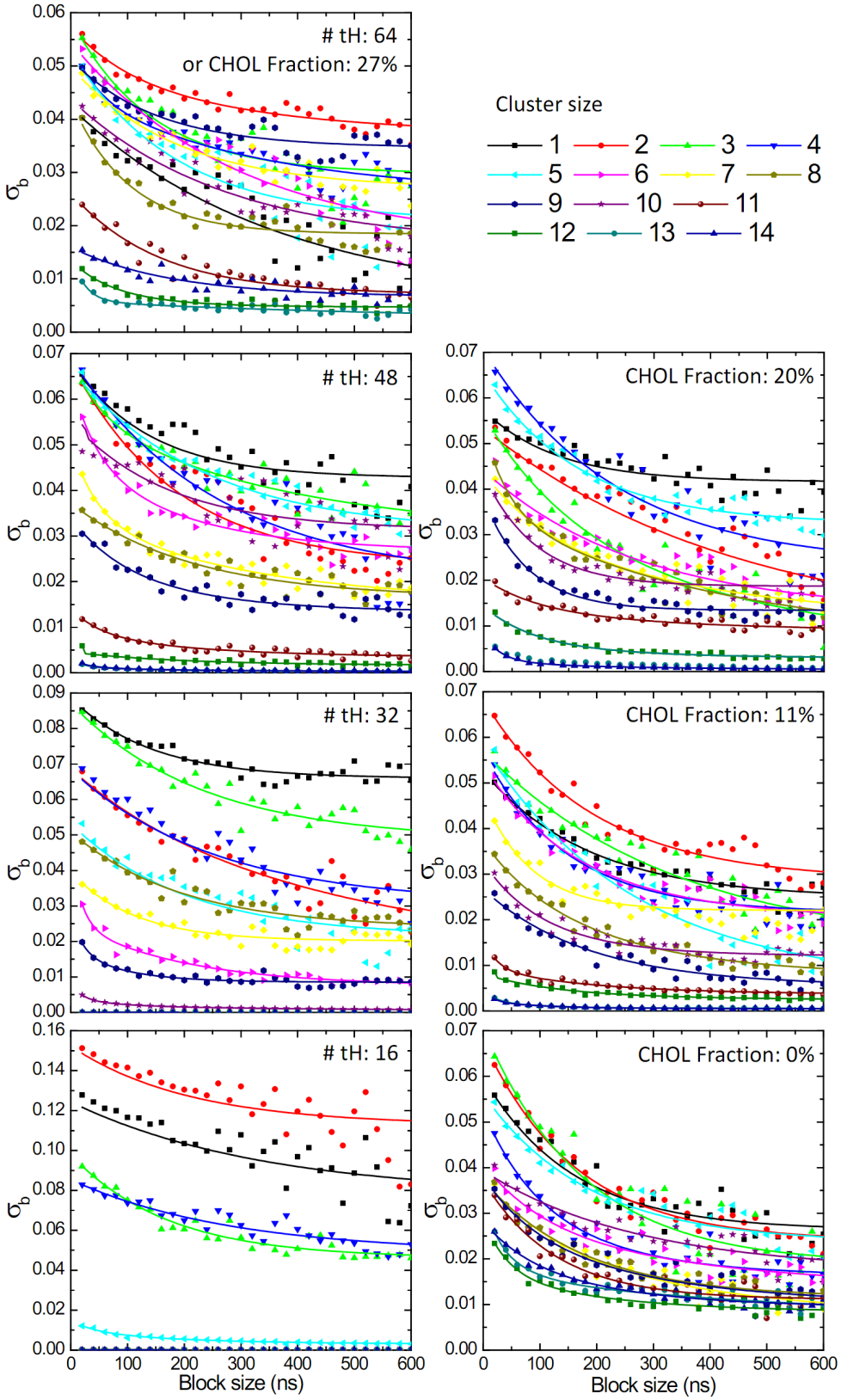

Figure S3. Error as a function of block size for different cluster sizes, calculated using equation 1 (lines represent exponential fits using the equation $y = y_0 + A_1 e^{-(x-x_0)/t_1} + A_2 e^{-(x-x_0)/t_2} + A_3 e^{-(x-x_0)/t_3}$).

5. Stability of H-Ras lipid anchor nanoclusters

In order to estimate the characteristic time scales of molecular exchange among nanoclusters or between nanoclusters and the non-clustered fraction, we used an autocorrelation function $f(t)$ defined as:

$$f(t) = \langle \frac{N(t_0) - N_{leave}(t_0+t)}{N(t_0)} \rangle_{t_0,n} \quad (2)$$

where $N(t_0)$ is the nanocluster size at time t_0 (t_0 representing the time point at which we begin following a given cluster), $N_{leave}(t_0 + t)$ is the number of molecules that leave the given cluster after a time lapse of t, n is the number of nanoclusters of size $N(t_0)$. When $t = 0, N_{leave}(t_0 + t) = 0, f(t) = 1$, the composition of the nanocluster is identical to the initial state. When $t \to \infty, N_{leave}(t_0 + t) \to N(t_0), f(t) \to 0$, the composition of the nanocluster is completely different from the initial state. In other words, $f(t)$ is the fraction of tH molecules that remain in the same initial cluster at time *t* relative to time t_o so that the speed with which $f(t)$ drops from 1 to 0 can be regarded as the decay rate of the given cluster. Additional details can be found in our previous reports[5, 6].

6. Effect of C60 on dynamics of membrane domains and H-Ras lipid anchor nanoclusters

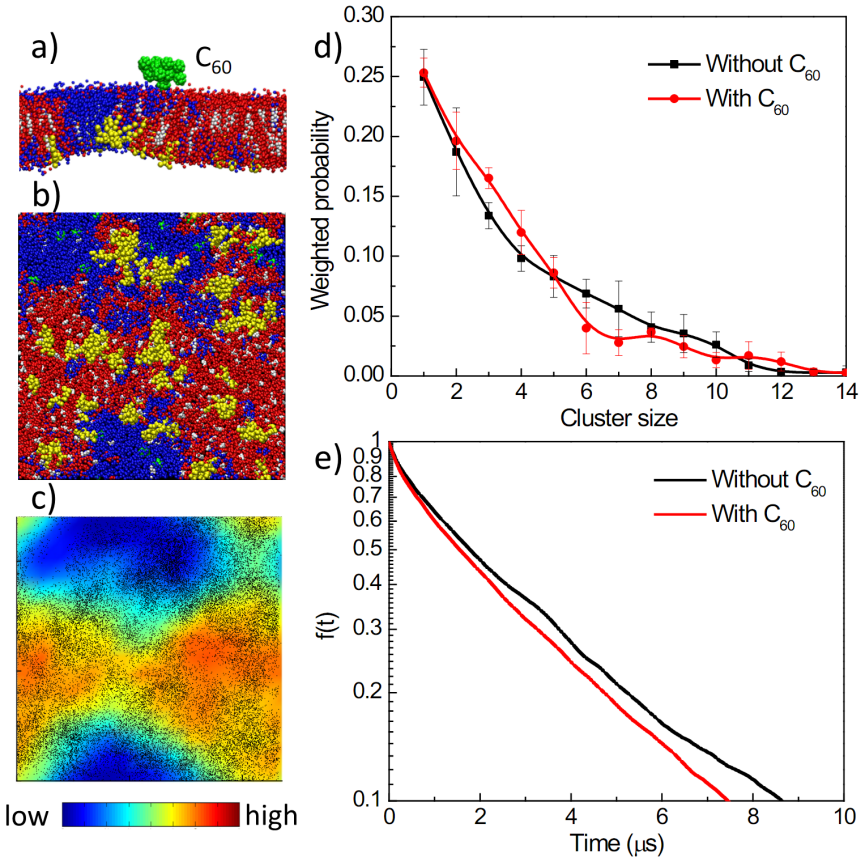

Figure S4**.** (a) Side-view of the initial system setup of C_{60} and tH nanoclusters (C60 is in green; color scheme for the rest of the molecules is the same as in main text Fig. 1). (b) Bottom-view of the last snapshot. (c) Two-dimensional normalized DPPC number density with the black points representing the location of tH. (d) Effect of C_{60} on tH nanocluster size distribution. e) Effect of C_{60} on tH nanocluster dynamics.

7. Comparison of tH clustering and dynamics upon depletion (current work) and increase (previous work) of peptide/cholesterol content.

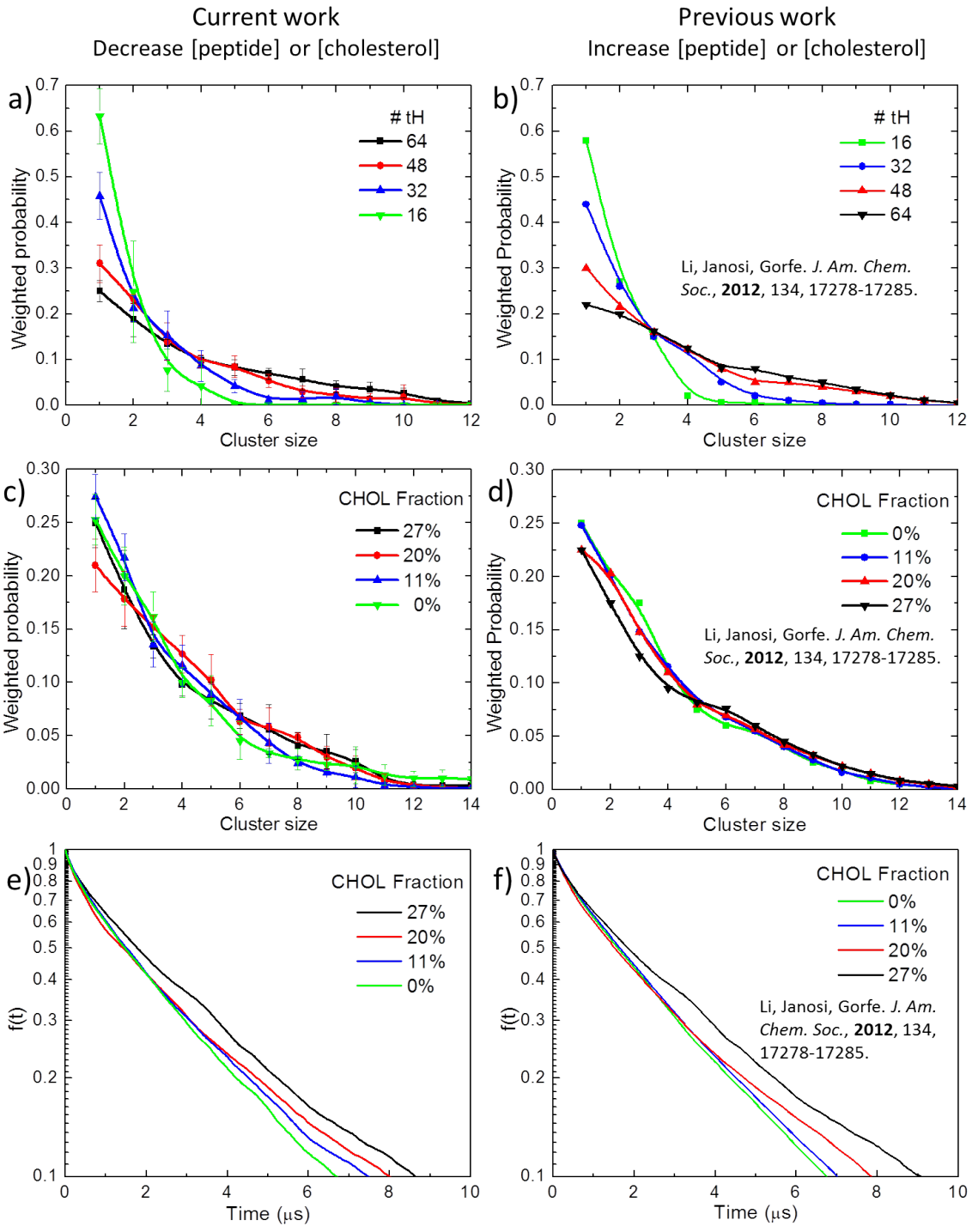

Figure S5. Reversible effects of decreasing and increasing peptide/cholesterol concentrations on tH nanocluster size distribution (a-d) and stability (e and f, for cluster size 6).

8. Results of two additional replicates of the simulations listed in Table 2.

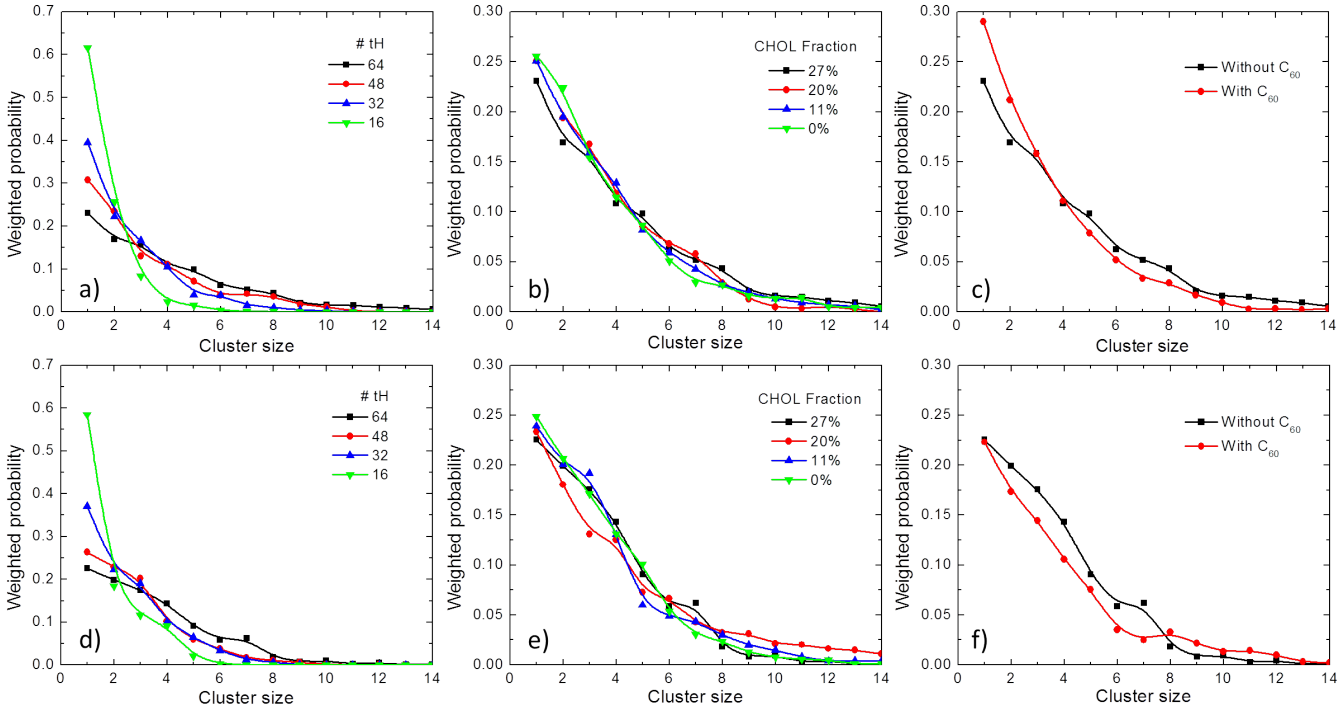

Figure S6. tH nanocluster size distribution from two replicates of each of the simulations listed in Table 2: (a, d), simulations with decreasing tH fraction; (b,c) simulations with decreasing cholesterol fraction; (c, f) simulations in the presence of the C60 nanoparticle. Note that the data in the two top left panels are also shown as inset in Figs. 1 and 2 of the main text.

Supporting References:

1. Z. Li and A. Gorfe, *Soft Matter*, 2013, **9**, 11249-11256.
2. S. Park, A. H. Beaven, J. B. Klauda and W. Im, *J. Chem. Theory Comput.*, 2015, **11**, 3466-3477.
3. A. Vogel, G. Reuther, K. Weise, G. Triola, J. Nikolaus, K. T. Tan, C. Nowak, A. Herrmann, H. Waldmann and R. Winter, *Angew. Chem. Int. Ed.*, 2009, **48**, 8784-8787.
4. A. Vogel, C. P. Katzka, H. Waldmann, K. Arnold, M. F. Brown and D. Huster, *J. Am. Chem. Soc.*, 2005, **127**, 12263-12272.
5. L. Janosi, Z. Li, J. F. Hancock and A. A. Gorfe, *Proc. Natl. Acad. Sci. U. S. A.*, 2012, **109**, 8097-8102.
6. Z. Li, L. Janosi and A. A. Gorfe, *J. Am. Chem. Soc.*, 2012, **134**, 17278-17285.
7. S. J. Marrink, H. J. Risselada, S. Yefimov, D. P. Tieleman and A. H. De Vries, *J. Phys. Chem. B*, 2007, **111**, 7812-7824.
8. G. Bussi, D. Donadio and M. Parrinello, *J. Chem. Phys.*, 2007, **126**, 014101.
9. M. Parrinello and A. Rahman, *J. Appl. Phys.*, 1981, **52**, 7182-7190.
10. J. C. Gower and G. Ross, *J. R. Stat. Soc. Ser. C-Appl. Stat.*, 1969, **18**, 54-64.
11. Z. Li and E. E. Dormidontova, *Soft Matter*, 2011, **7**, 4179-4188.
12. M. V. Gudheti, N. M. Curthoys, T. J. Gould, D. Kim, M. S. Gunewardene, K. A. Gabor, J. A. Gosse, C. H. Kim, J. Zimmerberg and S. T. Hess, *Biophys. J.*, 2013, **104**, 2182-2192.